A Constrained Molecular Dynamics (CoMD) study of nuclear near-ground-state properties

T. Depastas[1], *G.A.* Souliotis[1,*], *K.* Palli[1], *A.* Bonasera[2,3], and *H.* Zheng[4]

[1]Department of Chemistry, National and Kapodistrian University of Athens, Athens, Greece
[2]Cyclotron Institute, Texas A&M University, College Station, Texas, USA
[3]Laboratori Nazionali del Sud, INFN, Catania, Italy
[4]School of Physics and Information Technology, Shaanxi Normal University, Xi'an, China

Abstract. The Constrained Molecular Dynamics (CoMD) model is used to describe the properties of nuclear systems near the ground state. A procedure for global optimization of the initial configurations of the nuclei is developed. In addition, the neutron skins of various nuclear systems are calculated. Finally, the GDR and GMR spectra of medium-mass nuclear systems are studied. The effect of the model parameters to the spectra is explored. We conclude that an increased compressibility of $K = 308\ MeV$ results in increased GDR energy and decreased skin, while the total energy and the GMR energy remain almost unaltered.

1 Introduction

The nuclear N-body problem is intricate due to the underlying complicated nuclear interaction. The properties of the resulting low lying states have been studied with a wide variety of methods. These methods include various mean-field approaches, such as Skyrme-Hartree-Fock (SHF) [1] and semiclassical quantum and antisymmetrized molecular dynamics (QMD & AMD) models [2–4]. In recent years, the Constrained Molecular Dynamics (CoMD) model has been used to describe numerous phenomena of low-energy dynamics. Some examples incorporate studies of near Fermi energy reactions and fission of heavy nuclei [5]. The CoMD model forms the basis of the present work and some of its details are presented in the next section.
In this work we study some important near ground state properties of several nuclei. These properties include the neutron skin, radial density, GDR and GMR spectra. The organization of the paper is as follows. First the theoretical framework and computational details of the model are given. Then, we present a study of the initial configurations and the optimization process. After that, we approach the problem of the Giant Resonances. In particular, the Giant Dipole and Giant Monopole Resonances, along with the corresponding soft modes for several nuclear systems, are presented.

2 Theoretical Framework

The CoMD model is based on an effective two-body interaction with Skyrme potential characteristics, as described in [3, 5], with two-body potential terms as follows

$$V_{vol} = \frac{T_0}{\rho_0}\delta\left(\boldsymbol{r_i} - \boldsymbol{r_j}\right), \tag{1}$$

$$V_3 = \frac{2T_3\rho^{\sigma-1}}{(\sigma+1)\rho_0^{\sigma}}\delta\left(\boldsymbol{r_i} - \boldsymbol{r_j}\right), \tag{2}$$

$$V_{sym} = \frac{a_{sym}}{\rho_0}\delta\left(\boldsymbol{r_i} - \boldsymbol{r_j}\right)\left(2\delta_{\tau_i,\tau_j} - 1\right), \tag{3}$$

$$V_{sur} = \frac{C_s}{\rho_0}\nabla^2_{\langle\vec{r}_i\rangle}\delta\left(\boldsymbol{r_i} - \boldsymbol{r_j}\right), \tag{4}$$

$$V_{coul} = \frac{e^2}{\left\|\boldsymbol{r_i} - \boldsymbol{r_j}\right\|} \tag{5}$$

In the above relations, V_{vol} corresponds to the volume term, V_3 to the three-body term, V_{sym} to the symmetry term, V_{sur} to the surface term, while V_{coul} describes the Coulomb repulsion of the protons. The parameters ρ_0, a_{sym} and C_s are the saturation density, the symmetry and surface parameter, respectively. These are fixed to $\rho_0 = 0.165\ fm^{-3}$, $a_{sym} = 32\ MeV$ and $C_s/\rho_0 = -1$, unless otherwise stated. The constants T_0, T_3 and σ are related to the compressibility of nuclear matter (NM) and are determined by the enforcement of the saturation condition of NM with the use of the effective interaction with terms as in eq. (1–5), as described in [3]. The trial one-body wavefunctions that are used in the model, are Gaussian wave-packets and, in the Wigner representation, have the form

$$f_i(\boldsymbol{r}, \boldsymbol{p}) = \frac{1}{\left(2\pi\sigma_r\sigma_p\right)^3} e^{-\frac{(r-\langle r_i\rangle)^2}{2\sigma_r^2}} e^{-\frac{(p-\langle p_i\rangle)^2}{2\sigma_p^2}} \tag{6}$$

The σ_r and σ_p are the widths, while $\langle\boldsymbol{r}_i\rangle$ and $\langle\boldsymbol{p}_i\rangle$ are time dependent centroids of the wave-packet of nucleon i in phase space. In the calculations presented below,

*e-mail: soulioti@chem.uoa.gr

$\sigma_r = 1.30\ fm$ and $\sigma_p = \hbar/2/\sigma_r$, unless stated otherwise. The application of the Time Dependent Variational Principle (TDVP) to the Lagrangian of the model with the wavefunctions of eq. (6) leads to the Hamilton's equations of motion in the Wigner representation.

The many-body wavefunction of the model is considered to be a direct product of the one-body wavefunctions of eq. (6). The Pauli Principle is enforced in the model through a constraint of the phase space volume of each nucleon and through Pauli-blocking of nucleon-nucleon (NN) scattering. The total occupation fraction of a phase space hypercube with volume h^3 is constrained through

$$\bar{f}_i = \sum_{j \subset L} \delta_{\tau_i,\tau_j} \delta_{s_i,s_j} \int_{h^3} f_j(\boldsymbol{r},\boldsymbol{p})\, d^3r d^3p \leq \frac{paulm}{128} \qquad (7)$$

where L is an ensemble of nucleons j neighboring i. The parameter *paulm* signifies the strength of the Pauli correlations. Higher *paulm* values result in less strict enforcement of the Pauli Principle.

3 Computational Details

In our computational procedure, every calculation with CoMD consists of three steps, the initialization, the evolution and the data processing. The collection of the phase space centroids for each nucleon make up the initial nuclear configuration. These configurations result from a Monte Carlo Simulated Annealing algorithm, that minimizes the total energy of the nucleus. This process takes place in the initialization step [6, 7].

After an initial configuration is chosen, the nucleus evolves for a determined time interval. To account for the approximate character of the equations, before the evolution, the phase space centroids are randomly rotated. This rotation respects the conservation of energy and angular momentum and produces a set of different possible nucleon trajectories in phase space. Each of these is defined as an "event". The aforementioned calculations comprise the evolution step.

The final step depends on the nuclear phenomenon that is studied. First, the nucleon trajectories for each event are properly averaged. Then, we extract information regarding various nuclear properties, such as the mass density or the neutron skin. In order to study the Giant Resonances (GR), one must transform a nuclear property from the time to the frequency domain. This property forms the response function and the transformation is achieved through the use of a Fast Fourier Transform (FFT) code.

4 Initial Configurations and Ground State Properties

4.1 Global Optimization Algorithm

The initialization algorithm produces a set of various possible initial configurations, as described in the previous section. Thus, the question regarding the choice of the initial configuration arises naturally. Each configuration is characterized by the total energy per nucleon, the mass radius and average density and *paulm* parameter. In some of our previous works, the configurations with minimum energy per nucleon have been chosen for the evolution calculation. Another option would be the use of configurations with energies near the experimentally measured value of the binding energy. Both approaches can yield good predictions for the dynamical aspects of reactions and other nuclear phenomena, but usually have higher radii and lower densities than expected.

When one of the characteristics of the initial configurations is improved, the other characteristics become worse. To settle this problem, we developed an algorithm for global optimization of the configurations. In the algorithm, these "optimum" states are chosen based on the values of total energy per nucleon, rms radius, average density and occupation fraction. For the relative error evaluation, the experimental binding energies [8] are used along with the *paulm* values for the occupation fractions. Additionally, the radius choices are evaluated according to the formula $R = 1.2A^{1/3}$. The nuclei tend to shrink in the evolution code, with lower radii that are closer to the experimental value, rather than the empirical one. Finally the average densities are evaluated according to their proximity to Skyrme-Hartree-Fock (SHF) calculations. The evaluation process is performed by a dedicated code that extracts the configurations according to aforementioned criteria.

4.2 Ground State Properties and the Effect of Model Parameters

In the present work, we used the optimum configurations to study the properties of the nuclear ground states, such as the total energy per nucleon. We note that the model reproduces the experimental values for the energies with fair accuracy, while it predicts higher values for the average radii.

The radial density is another property that was studied. The optimum states yield improved densities, that have close proximity with those calculated by SHF mean-field approaches. In figure 1 the mass densities (top row), the proton densities (central row) and the neutron densities (bottom row) of ^{40}Ar (left) and ^{64}Ni (right) are plotted against the radial coordinate. The CoMD calculated density is represented by a continuous line, while the dashed line corresponds to the SHF density. In the present preliminary calculations, the approximate treatment of the Pauli principle and the gaussian profile of the wavepacket result in a dip in the nuclear density at low radii that we expect to remove in subsequent calculations.

To understand the dependence of the equation of state (EOS) on the parameters of the effective interaction, we studied total energies, radii, average densities and occupation fractions of the optimum configurations. In figure 2 we show the variation of the minimum energy per nucleon of the ^{68}Ni configuration space with respect to the *paulm* parameter (a), compressibility (b), saturation density (c) and effective mass ratio (d). These parameters and their effects are discussed in the following paragraphs.

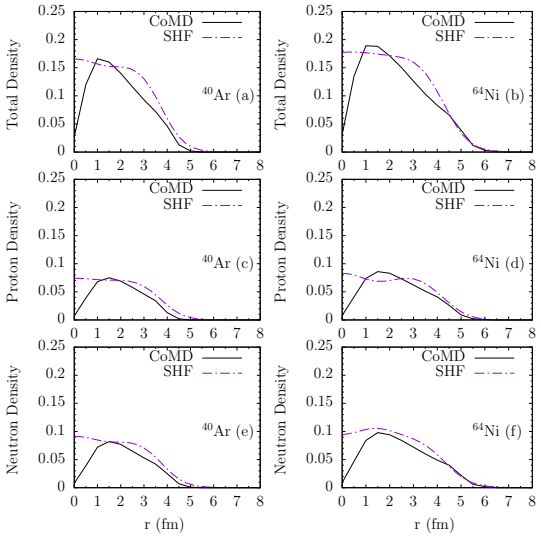

Figure 1. Radial densities of ^{40}Ar (left column) and ^{64}Ni (right column) plotted against the radial coordinate. The top row gives the plots of the total density, the middle row of the proton density and the bottom row of the neutron density. The solid black line corresponds to the CoMD calulation and the purple dashed line to the SHF calculation.

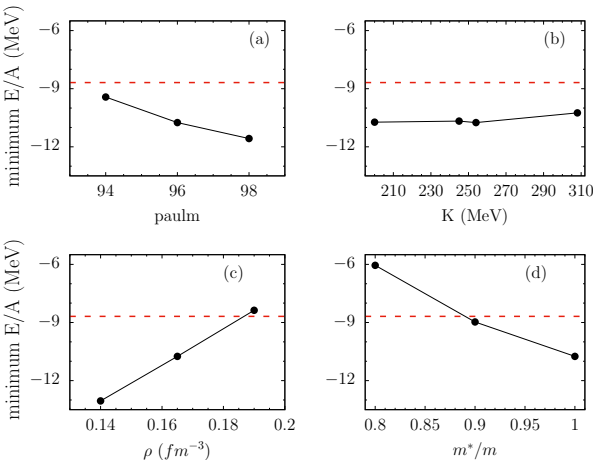

Figure 2. Minimum Energy per nucleon of ^{68}Ni plotted against paulm (a), compressibility (b), saturation density (c) and effective mass ratio (d). The points connected with the solid black lines correspond to the CoMD calulation and the red dashed line to experimental data from [8].

The *paulm* parameter determines the strength of the Pauli Principle, as it is already discussed. The smaller values increase the radius and decrease the average density of the nucleus. Additionally, the energy of the system is increased, as seen in figure 2(a). This is understood to be a consequence of the degeneracy pressure of a Fermi Gas. Thus, mostly the kinetic part of the Hamiltonian contributes to the increase of the energy. We wish to comment that the enforcement of the Pauli principle in CoMD via the constraint corresponds to a purely quantal effect and may correspond to the emergence of shell effects in the energy spectrum of the system. We have made such a preliminary exploration, but we do not discern energy gaps corresponding to shells in our calculations. In this vein, the possibility of including a spin-orbit term in the potential will also be explored.

The compressibility K is an important parameter of the EOS, that signifies the response of the nuclear system to compression. For the effective interaction of the CoMD model (eq. 1–5), it can be expressed as:

$$K = 9T_3 \frac{\sigma(\sigma-1)}{(\sigma+1)} - 2\bar{\epsilon_F} \tag{8}$$

where $\bar{\epsilon_F}$ is the average Fermi energy of NM. As expected, the increase of the compressibility results in a decrease of the radius and an increase of the density. Interestingly, the energy of the system seems to be independent of the compressibility choice, as seen in figure 2(b). This results from a simultaneous increase of the kinetic component and a decrease of the potential component of the Hamiltonian.

The saturation density (ρ_0) of the system signifies the maximum density of a nucleus and results from the repulsive part of the effective interaction. As shown in 2(c), this parameter is proportional to the system's energy. Another important characteristic of the nuclear interaction is the inclusion of momentum dependent terms. These terms represent the finite range of the interaction. In the current version of the model, we include the momentum dependence in the low energy limit, as an effective mass (m^*). The smaller effective mass results in an increase of the kinetic energy of the system, and thus to an increase of the total energy. This tendency can be clearly seen in figure 2(d). In the discussion below, the effective mass is $m^* = m$, unless otherwise stated.

4.3 Neutron Skin Calculations

The neutron rich nuclei are stabilized by distributing the excess of neutrons near the nuclear surface that is distinct from the N=Z symmetric core. This extends the neutron density further from the proton density by a few tenth of fm, creating the characteristic neutron skin (r_{np}), expressed as the difference of the rms radii of protons and neutrons. The neutron skin of various nuclides has been investigated with both theoretical and experimental approaches [4]. The CoMD model generally predicts neutron skins with higher values, compared to experimental data or empirical expectations. In general, increased compressibility and *paulm* result in decreased values for the skin. We report herein, that the ^{208}Pb calculation with $K = 254$ MeV, $paulm = 102$ and $m^*/m = 1$ yields 0.43 fm neutron skin, somehow higher than the experimental value of $0.33^{+0.16}_{-0.18}$ fm.

The neutron skin, of course, depends on the relative number of protons and neutrons, that may be expressed by the isospin asymmetry factor, $m_\chi = \frac{N-Z}{A}$. As described in [4], the neutron skin depends linearly on the isospin asymmetry. In figure 3, we present the correlation of the neutron skin with the m_χ for various isotopic and isobaric chains of medium-mass nuclei. The negative neutron skin values correspond to proton-rich nuclei, as expected. The

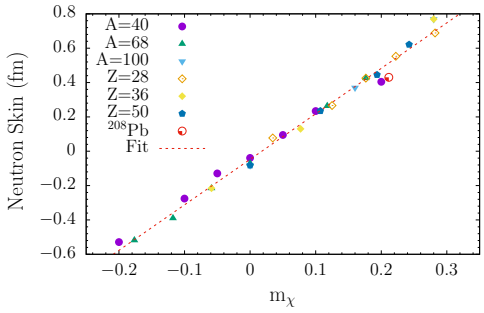

Figure 3. Neutron skin plotted against the isospin asymmetry parameter. The points represent CoMD calculations of various isotopic and isobaric chains, according to the key. The dashed red line represents our linear fit, eq. (9).

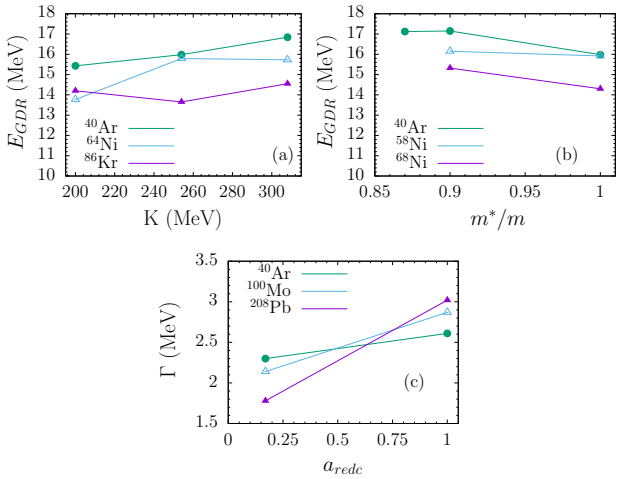

Figure 4. Effects of important model parameters to the GDR spectrum of various nuclides, according to the key. The top row presents the variation of the GDR energy with respect to compressibility (a) and effective mass ratio (b). The bottom panel (c) shows the variation of the width with respect to the reduction parameter of the NN scattering cross section.

calculations shown in fig. 4 are fitted with the formula

$$r_{np} = (2.65 \pm 0.051)\, m_\chi + (-0.047 \pm 0.081) \qquad (9)$$

5 Isovector Giant Dipole Resonances

The Giant Resonances (GR) are some of the most interesting phenomena of nuclear dynamics. They consist of several collective modes of motion, that can be considered as multipole excitations of the nuclear radius. By studying these resonances, one can extract useful information with regard to the EOS and effective interaction.
In this work, we study the Isovector Giant Dipole (IVGDR or GDR). This is in effect the off-phase oscillation of the proton and neutron fluids, around their equilibrium positions. This resonance is one of the most thoroughly investigated GRs (e.g. [7, 11**?**]). It has been described by a wide variety of theoretical and computational methods ranging from liquid-drop and BUU approaches [9] to RPA and TDHF [8].

5.1 Theoretical Framework and the Effect of Model Parameters

In this study, the GDR problem is approached as follows. We consider an initial perturbation of the nucleon centroids in either cartesian or momentum space. The coordinate space perturbation affects the nucleon's z-coordinate, while conserving the center of mass of the system. The momentum space perturbation consist of a quadrupole perturbation of the Fermi sphere that conserves the total volume in momentum space. Both these perturbations induce the GDR effect. The spectrum is extracted by the Fourier transform of the distance between the centers of mass of protons and neutrons. In the coordinate space, the z-axis perturbation is defined as $D = \frac{A}{Z} d_n = \frac{A}{N} d_p$, where d_n, d_p are the neutron and proton perturbations respectively.

By considering only the variation of the symmetry term in the low energy limit, we constructed a simple model in order to understand the dependencies of the full CoMD model. The corresponding collective equations of motion represent the damped GDR oscillation and their solution gives the following approximate relation for the centroid energy

$$E_{GDR} \approx \sqrt{\frac{A}{NZ} \frac{a_{sym}\rho_{np}}{m\rho_0\sigma_r^2}} \qquad (10)$$

where ρ_{np} is the neutron-proton interaction density.

In figure 4, we present the effect of the compressibility (a) and effective mass (b) to GDR energy, for a few nuclei. The increased compressibility corresponds to higher 3-body interaction (eq. 8) and yields nuclei with a more bound potential well. The main contribution to the GDR energy comes from the variation of the nuclear potential, thus higher compressibility values yield higher energy centroids. This can be seen in figure 4 (a). Additionally, the momentum dependence has a major role in the determination of the GDR [4]. In the approximation of eq. (10), the mass is present in the denominator. Thus lower effective mass yields higher GDR energies, a tendency that is confirmed in figure 4 (b).

The width of the GDR spectrum is mostly determined by the NN scattering cross section. In the CoMD model, the in-medium NN scattering cross section is approximated as the free cross section times a reduction parameter. In our implementation, this factor can have a constant value or it can be parameterized as [10]:

$$a_{redc}\,(T_{cm}, \overline{\rho}) = e^{-a_R \frac{\overline{\rho}/\rho_0}{1+(T_{cm}/T_0)^2}} \qquad (11)$$

where $T_0 = 150MeV$ and $a_R = 1.8$. For the present study, we may set $\overline{\rho} \approx \rho_0$ and $T_{cm} \ll T_0$, to obtain $\langle a_{redc} \rangle \approx 0.17$. The reduction parameter is given by eq. (11) in the following calculations, unless stated otherwise. In figure 4 (c) the width is plotted against the reduction parameter for different nuclei. As expected, increased cross section values result in increased GDR widths.

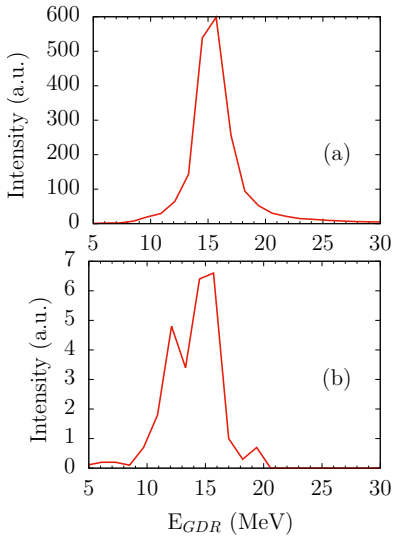

Figure 5. GDR spectra of ^{68}Ni. The top panel (a) represents the GDR response in cartsian space and the bottom (b) represents the momentum space response.

Apart from GDR, other isovector modes may be present in the model's isovector spectrum. The most important is the Pygmy resonance, with corresponds to an off-phase oscillation of the neutron skin of a neutron rich nucleus against its symmetric core. In the CoMD model, a momentum space perturbation can excite these soft degrees of freedom. In figure 5 we present the r-space (a) and p-space (b) GDR spectrum of ^{68}Ni for $K = 308\ MeV$. We note that the main peak at 15 MeV corresponds to the GDR and is lower by 2 MeV from the experimental value, of 17.84 MeV [13]. On the other hand, we may identify the secondary peak at 12 MeV as the Pygmy resonance. This is close to the experimental value of 11 MeV [13].

5.2 Isotopic and Isobaric Results

It is known that an effective interaction with an approximate treatment of the momentum dependence, appears to underestimate the GDR energies [4]. In figure 6, we present the variation of the GDR energy with mass number A. The dashed red curve corresponds to an experimental parameterization [4]. The points connected with lines show calculations with two EOS. The green points correspond to the standard "soft" EOS with $K = 254\ MeV$, $m^*/m = 1$ and $a_{sym} = 32\ MeV$, while the cyan points correspond to a "hard" EOS with $K = 308\ MeV$, $m^*/m = 0.9$ and $a_{sym} = 38\ MeV$. The soft EOS calculations differ from the experimental values by $3-4\ MeV$, while this energy gap becomes somewhat narrower for the hard EOS. We wish to comment here that the above tendency to favor larger K values does not agree with results supporting a softer EOS with K~250 (e.g. [14]). We think that the inclusion of a proper momentum dependence in the effective interaction of the CoMD model may reconcile this issue and is one of our future goals.

In the literature, empirical expressions for the GDR energy usually do not contain an explicit dependence on the isospin asymmetry (e.g. [4, 11, 12]), as the observed isospin effects are rather small. Here we confirm this behavior, but we note some decreasing trend for the neutron rich $m_\chi > 0$ nuclei. This can be seen in figure 7, where we show the variation of the GDR energy with respect to A, for different isotopic chains (a) and with respect to Z, for different isobaric chains (b).

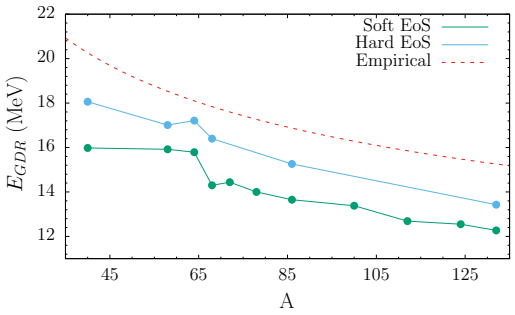

Figure 6. GDR energies of various nuclides with respect of the mass number. The green curve represents the soft EOS calculations, the cyan the hard EOS calculations and the red curve is an experimental parameterization from [4].

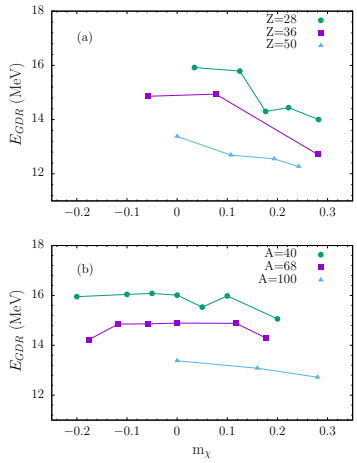

Figure 7. GDR energies plotted against the isospin asymmetry parameter. The top panel (a) shows the variation of various isotopic and the bottom (b) of various isobaric chains, according to the key.

6 Isoscalar Giant Monopole Resonances

The Isoscalar Monopole Resonance (ISGMR or GMR) is another important GR. It consists of the in-phase breathing mode of both neutrons and protons. This GR can constrain the compressibility of EOS and give important information regarding the effective interaction. Additionally, there exists a soft monopole mode for neutron rich nuclei, analogous to the Pygmy resonance. This GR corresponds to an isoscalar breathing mode of the neutron skin against the symmetric core.

In the CoMD model, the isoscalar modes are studied via a monopole perturbation in momentum space. The spectrum results from an FFT of the nuclear rms radius.

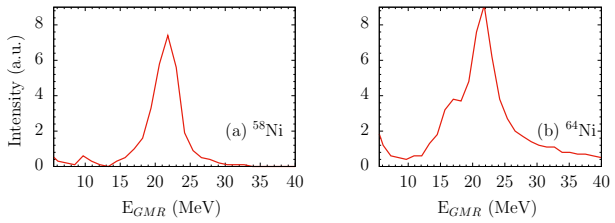

Figure 8. GMR spectrum of ^{58}Ni (a) and ^{64}Ni (b). Both are extracted by an momentum space GMR perturbation.

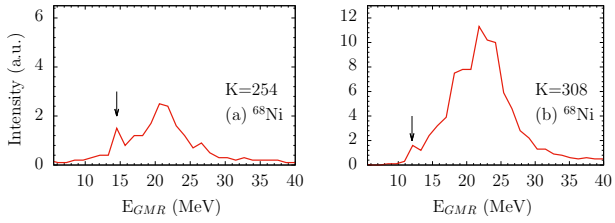

Figure 9. GMR spectrum of ^{68}Ni for two different compressibilities. The left panel (a) represents K=254 MeV and the right panel (b) represents K=308 MeV calculation. The soft monopole mode is indicated by an arrow.

In this work, we studied the isoscalar response of ^{A}Ni isotopes, with $A = 58, 64, 68$. In figure 8 we present the GMR spectrum of ^{58}Ni (a) and ^{64}Ni (b). Furthermore, in figure 9 we present the GMR spectrum of ^{68}Ni with $K = 254$ MeV (a) and $K = 308$ MeV (b). We note that, the main GMR peak of the nickel isotopes is found at 21.5 MeV , which is close to the experimental value of 21.1 ± 1.9 MeV [15]. As for the ^{68}Ni isotope, the soft monopole appears at 14.5 MeV, which is also near the experimental value of 12.9 ± 1.0 MeV [15]. An interesting observation regarding the effect of the compressibility can be made from figure 9. The increase of K from 254 MeV to 308 MeV leads to larger total cross section (strength) of the peak and an increase of the GMR centroid by ~ 1 MeV. Finally, the soft mode peak retains its strength and width, while the width of the main GMR peak is increased.

7 Discussion and Conclusions

In this work, we used the CoMD model to describe properties of nuclear systems near the ground state. First, we developed a procedure to choose an initial phase-space configuration with optimum characteristics. Furthermore, we studied the effective interaction and the effect of its parameters. We found that an increased compressibility results in an increased GDR energy and decreased skin, while the total energy and the GMR energy remain almost unaltered. The neutron skins of various nuclei were calculated. Our CoMD calculations appear to overestimate the skin compared to empirical values or experimental results.

An important part of our work was devoted to the study of GDR. In the CoMD model, the GDR energy is underestimated by a few MeV. These results can be partially improved by choosing a "harder" EOS with $K = 308$ MeV. The GDR can be improved further by the inclusion of a momentum dependent interaction, that we plan to do in the near future. Finally, it appears that our CoMD results agree better with the experimental values, as the mass of the nuclear system increases. This suggests that the CoMD model in its current implementation provides overall better results for heavier nuclei.

8 Acknowledgement

Financial support for this work was provided by the Special Account for Research Grants of the National and Kapodistrian University of Athens. AB and HZ were supported by the U.S. Department of Energy under Grant No. DE-FG03-93ER40773 and NNSA Grant No. DENA0003841 (CENTAUR).

References

[1] D. Vautherin, D.M. Brink, Phys. Rev. C **5**, 3 (1971).
[2] Y. Kanada-En'yo, M. Kimura, A. Ono, Prog. Theor. Exp. Phys. **1**, 202 (2012).
[3] M. Papa, T. Maruyama, A. Bonasera, Phys. Rev. C **64**, 024612 (2001).
[4] G. Giuliani, H. Zheng, A. Bonasera, Prog. in Part. and Nucl. Phys. **76**, 116 (2014).
[5] N. Vonta, G.A. Souliotis, M. Veselsky, A. Bonasera, Phys. Rev. C **92**, 024616 (2015).
[6] M Papa, J. Phys.: Conf. Ser. **420**, 012082 (2013).
[7] M. Papa, G. Giuliani, A. Bonasera., J. Comput. Phys. **208**, 403 (2005).
[8] J. L. Basdevant, J. Rich, M. Spiro, *Fundamentals in nuclear physics: From nuclear structure to cosmology* (Springer, New York, 2005).
[9] G. Bonasera, M. R. Anders, S. Shlomo, Phys. Rev. C **98**, 054316 (2018).
[10] R. Wang, Z. Zhang, et al Phys. Let. B **807**, 135532 (2020).
[11] S. Shlomo, G. Bertsch, Nucl. Phys A **243**, 507 (1975).
[12] J.S. Wang, W.Q. Shen et al, Eur. Phys. J. A **7**, 355 (2000).
[13] D.M. Rossi, et al, Phys. Rev. Lett. **111**, 242503 (2013)
[14] M. Veselsky et al, Phys. Rev. C **94**, 064608 (2016).
[15] X. Sun, Phys. Rev. C **103**, 044603 (2021).